High-resolution transmission electron microscopy investigation of a stacking fault in β-Si_3N_4

X. G. NING, D. S. WILKINSON, G. C. WEATHERLY
Department of Materials Science and Engineering, McMaster University, 1280 Main Street West, Hamilton, Ontario L8S 4L7, Canada

H. Q. YE
Laboratory of Atomic Imaging of Solids, Institute of Metal Research, Chinese Academy of Sciences, Wenhua Road 72, Shenyang 110015, People's Republic of China

High-resolution transmission electron microscopy images of stacking faults on (0 0 1) and ($\bar{1}$ 0 1) planes in a β-Si_3N_4 whisker were obtained and compared to image simulations. This procedure showed that the atomic structure of the four atomic planes around the (0 0 1) stacking fault plane in the β-phase is very similar to that of the unit cell of α-Si_3N_4 crystal. The stacking fault was observed to climb under electron irradiation in the microscope.

1. Introduction

Silicon-based ceramics are of great interest due to their high-temperature strength. They have lower thermal expansion coefficients than oxides, resulting in better thermal shock resistance. In recent years, silicon nitride ceramics have been toughened by increasing the length/diameter ratio of the β-Si_3N_4 grains [1]. Such a development is related to the α–β phase transformation and α-rich starting powders are required [2]. β-Si_3N_4 whisker-reinforced silicon nitride matrix composites can be now fabricated by *in situ* processing [3]. Thus, observations of the microstructures of silicon nitride ceramics are of particular importance in the context of high-temperature engineering applications. In this work, the atomic structure of a stacking fault found in β-Si_3N_4 whiskers is considered.

The crystal structure of α-Si_3N_4 is trigonal (space group P31c), with cell dimensions $a = 0.781$ nm and $c = 0.559$ nm [4]. There is still some argument about the crystal structure of β-Si_3N_4. The unit cell of β-Si_3N_4 is hexagonal with $a = 0.760$ nm and $c = 0.291$ nm [5]. The space group was determined as $P6_3/m$ from convergent-beam electron diffraction [6], or as $P6_3$ [7] by both convergent-beam electron diffraction and X-ray diffraction [5]. In the projected model of β-Si_3N_4 along [0 0 1], there is no difference between the structures of $P6_3$ and $P6_3/m$; they are distinguished only by a small displacement of the z coordinates of nitrogen atoms, approximately 0.005 nm [7]. In the present work, the analysis was based on a β-Si_3N_4 crystal with the $P6_3$ space group.

2. Experimental procedure

The β-Si_3N_4 whiskers were obtained from UBE Industries Co. Ltd, Japan. The diameter and the length of the whiskers were in the ranges 0.5–1.5 and 10–30 μm, respectively. The chemical composition of the 6061Al alloy was 0.8–1.2 wt % Mg, 0.4–0.8 wt % Si, 0.15–0.4 wt % Cu with the balance aluminium. The β-Si_3N_4/6061Al composite was fabricated by a squeeze-casting technique. Samples were studied in the as-fabricated state.

High-resolution transmission electron microscopy (HRTEM) observations were carried out in a Jeol 2000EX-II high-resolution transmission electron microscope (with an interpretable resolution of 0.21 nm at 200 kV operating voltage). The HRTEM image simulations were carried out using EMS software [8] on a Silicon Graphics workstation. The experimental conditions used for all the simulations were an accelerating voltage of 200 kV, a spherical abberation coefficient of 0.7 mm, a focus spread of 8 nm, a beam divergence of 0.75 mrad, a sample thickness of 2.3 nm, and a defocus of − 51 nm.

3. Results and discussion

Transmission electron microscope (TEM) observations showed that all the β-Si_3N_4 whiskers had a [0 0 1] growth direction, with the basic shape of a hexagonal prism (bounded by six {1 0 0} side surfaces and six very narrow {1 1 0} side surfaces) [9]. Some whiskers contained a small amount of α-Si_3N_4 and there was a specific orientation relationship between the α- and β-phases: $[0\,0\,1]_\alpha \| [0\,0\,1]_\beta$ and $[1\,0\,0]_\alpha \| [1\,0\,0]_\beta$ [10]. Two types of whiskers were found; fault-free, perfect whiskers, and faulted whiskers, containing stacking faults, dislocations and α-Si_3N_4 regions [11].

Fig. 1 shows HRTEM images of a stacking fault in β-silicon nitride, viewed along the [0 1 0] direction.

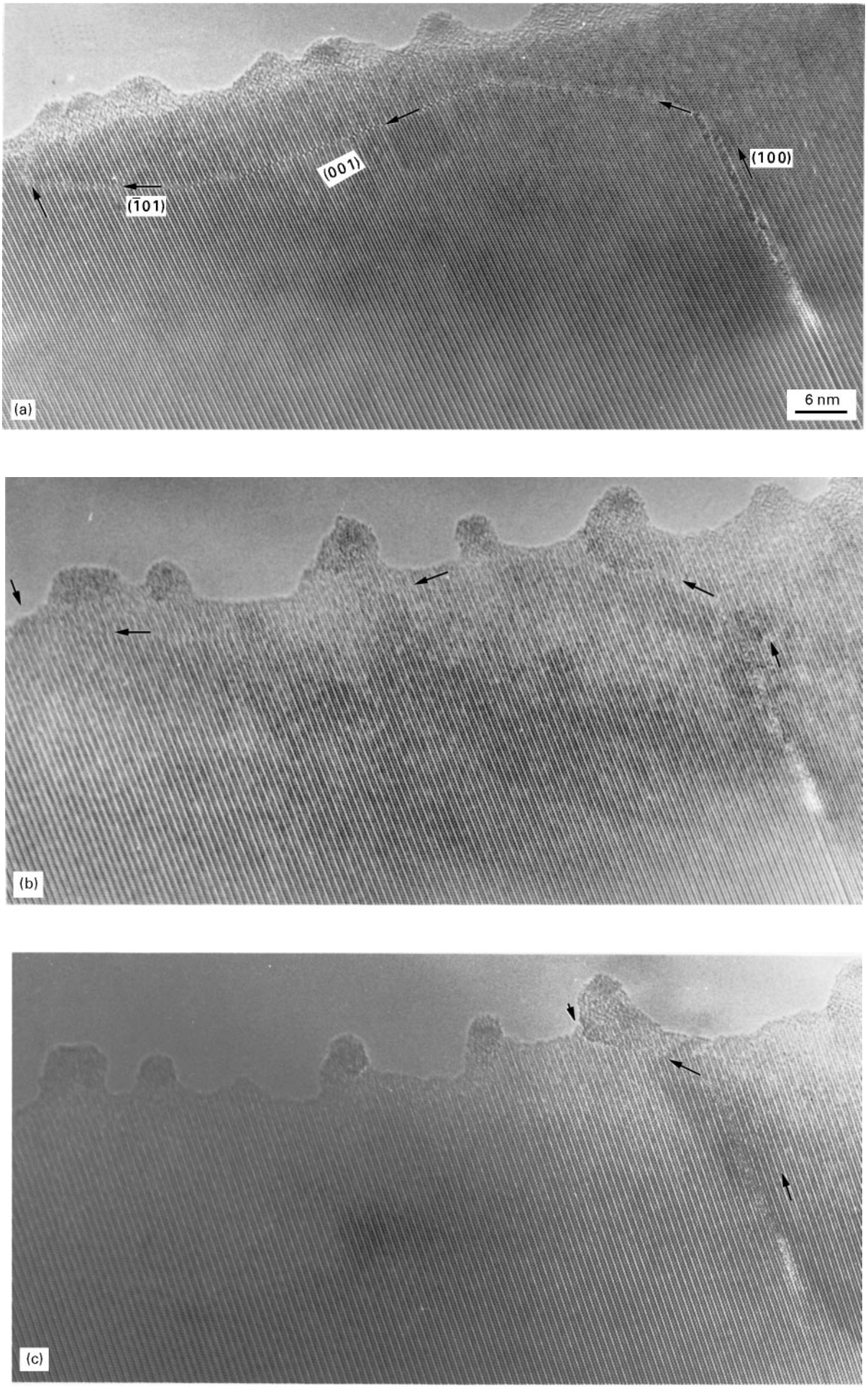

Figure 1 (a–c) HRTEM images of a stacking fault in β-Si_3N_4 taken at 5 min time intervals, showing apparent "climb" of the stacking fault under 200 keV electron irradiation.

The stacking fault lies principally on $(\bar{1}\,0\,1)$ and $(0\,0\,1)$ planes. The partial dislocation to the left of the stacking fault has already moved out of the surface, while the one on the right is located on the trace of the $(1\,0\,0)$ plane. Fig. 1a–c correspond to the same area, taken at time intervals of about 5 min. There is evidence of surface diffusion within the surface amorphous layer. In addition, the stacking fault moves towards the surface and has almost disappeared after 10 min. Detailed analysis of many images taken over this time period confirmed that the fault moved towards the free surface of the foil. For determining the translation vector of the stacking fault, the image around the $(0\,0\,1)$ stacking fault in Fig. 1a was enlarged and is shown in Fig. 2. The upper and lower parts of the crystal around the stacking fault were seen to be shifted one-sixth of the periodicity ($[2\,1\,0]$) along the $(0\,0\,1)$ plane, and half of the periodicity ($[0\,0\,1]$) normal to the $(0\,0\,1)$ plane. Considering all the possible translation vectors for stacking faults in a hexagonal structure, we found that the translation vector of the stacking fault in Fig. 1 was $[\bar{2}\,\bar{4}\,\bar{3}]/6$. A simulated image of β-Si_3N_4 along $[0\,1\,0]$ is inserted in Fig. 2, together with the unit cell, as seen in this projection. Fig. 3 shows the climb of the terminating partial dislocation at the right-hand side of the fault under the electron beam. The Burgers vector of the partial dislocation was also determined to be $[\bar{2}\,\bar{4}\,\bar{3}]/6$, i.e. it is a Frank sessile dislocation [12]. Frank partial dislocations cannot slip but can climb in a hexagonal system [12]. The exact mechanism responsible for the apparent climb of the fault, shown in Fig. 1, is not clear. In bulk crystals, stacking faults can only move in a direction normal to the fault plane by a combination of glide and climb processes associated with the motion of defects across the boundary plane. The defect in this case would have both step and dislocation character. Such a mechanism was not evident here, as the boundary moved in an apparently smooth fashion without recourse to defect propagation. We suggest that this is associated with electron-beam irradiation effects, but the precise nature of the process, as well as the origin of the force causing the fault to move, are obscure.

Generally, dislocations with Burgers vector of the type $[0\,0\,1]$ in hexagonal closed-packed (hcp) structures are unstable because they tend to dissociate according to the scheme [12]:

$$[0\,0\,\bar{1}] \rightarrow [\bar{2}\,\bar{4}\,\bar{3}]/6 + [2\,4\,\bar{3}]/6 \qquad (1)$$

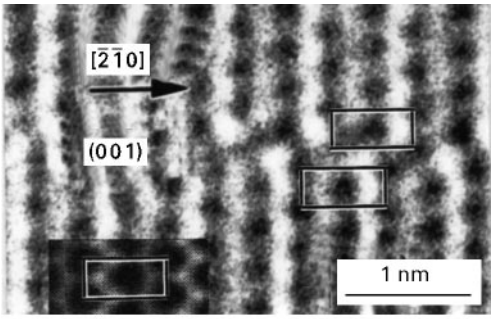

Figure 2 Enlarged HRTEM image of part of Fig. 1a. The insert shows the simulated image of β-Si_3N_4 as described in the text.

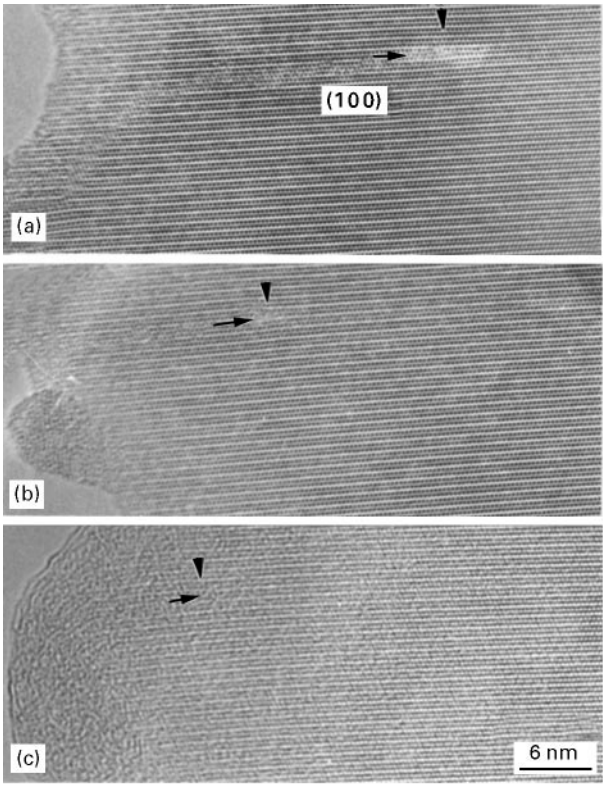

Figure 3 Climb of the partial dislocation in the stacking fault in Fig. 7, shown by HRTEM images. The position of the dislocation core is marked by arrows.

However, in β-Si_3N_4 crystals, such a dissociation is not energetically favourable because the c/a ratio of 0.38 is much smaller than the value of 1.63 found for ideal hcp structures; i.e. in this case

$$|\boldsymbol{b}_{[0\,0\,\bar{1}]}|^2 < |\boldsymbol{b}_{[\bar{2}\,\bar{4}\,\bar{3}]/6}|^2 + |\boldsymbol{b}_{[2\,4\,\bar{3}]/6}|^2 \qquad (2)$$

because

$$c^2 < (a^2/3 + c^2/4) + (a^2/3 + c^2/4) \qquad (3)$$

Thus, the dissociation of $[0\,0\,\bar{1}]$ has not been found in β-Si_3N_4 [13–16]. We suggest, therefore, that the stacking fault observed here was not created by a dislocation dissociation, but probably during the α–β phase transformation as part of the whisker growth process. The following analysis provides further support for this viewpoint.

Fig. 4 shows enlarged HRTEM images of the stacking fault on different planes. Fig. 5 shows the construction of the atomic structure used for image simulations of the stacking fault, where the larger spheres represent silicon atoms and the smaller ones represent nitrogen atoms. Fig. 5c shows the atomic projection of the α-Si_3N_4 crystal along a $[0\,1\,0]$ direction. The simulated image of β-Si_3N_4 along $[0\,1\,0]$ of the β-Si_3N_4 matrix is also inserted in Fig. 4b. The black dots on the image correspond to the atomic columns of silicon with high atomic density along $[0\,1\,0]$, while the bright dots or lines correspond to atomic columns of nitrogen surrounded by atomic columns of silicon, trigonally coordinated to the nitrogen. If we remove one $(0\,0\,1)$ atomic plane, such as the dashed plane in Fig. 5a, and then translate the crystal above the $(0\,0\,1)$ plane by $\langle\bar{1}\,\bar{2}\,0]\rangle/3$, the atomic structure of a stacking

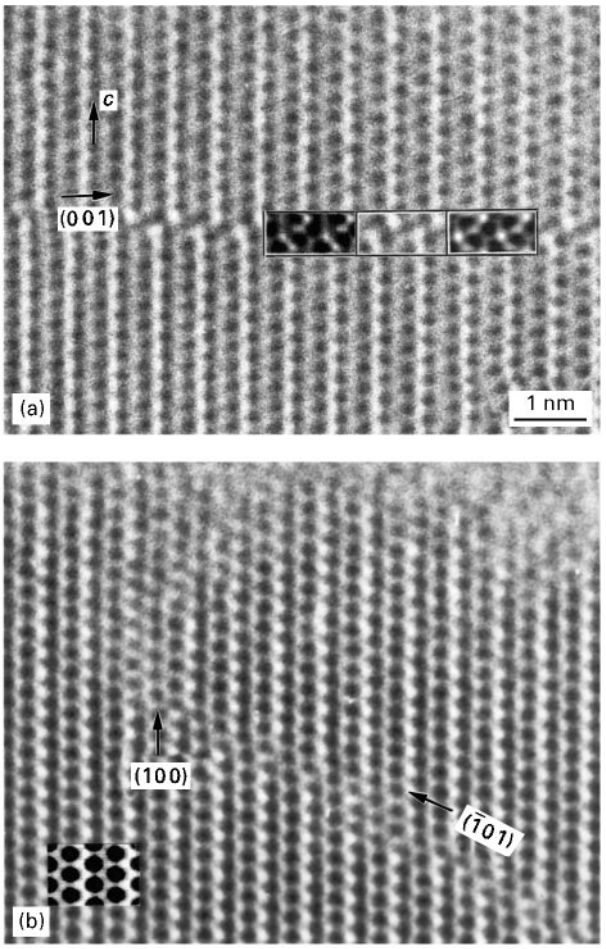

Figure 4 Enlarged HRTEM images of the stacking fault in Fig. 7 on (a) (0 0 1) and (b) ($\bar{1}$ 0 1) planes. The simulated images of the β-Si_3N_4 matrix (inserted in (a)), the stacking fault on the (0 0 1) plane (inserted in the centre of (b)) and the α-Si_3N_4 crystal (inserted on the right of (b)) are illustrated.

fault on the (0 0 1) plane shown in Fig. 5b is formed. The unit cell of the four atomic planes (i.e. the stacking fault unit (SFU) formed by the ABCD stacking sequence) is outlined in Fig. 5b. This is similar to the atomic structure of α-Si_3N_4 shown in Fig. 5c. Fig. 1 shows that the fault plane can change from (0 0 1) to ($\bar{1}$ 0 1) without introduction of defects at the junction of the (0 0 1) and ($\bar{1}$ 0 1) planes. Fig. 6 illustrates this schematically. We have used this model to simulate the lattice images of the faults on the (0 0 1) and ($\bar{1}$ 0 1) planes. Fig. 7a shows the simulated image of the stacking fault using the model of Fig. 5b. Very good agreement exists with the experimental image. The image of the fault can be equally well represented by using the α-Si_3N_4 cell. This is shown by the insert in Fig. 4a, where the outlined unit cell for α (Fig. 5c) has been used in the simulation in the inserted simulated image on the right of Fig. 4a. The inserted simulated image on the left of Fig. 4a corresponds to the atomic structure of the stacking fault in Fig. 5b. Good agreement is seen to exist between the two simulated images and the experimental image of the stacking fault. Therefore, to a first approximation, the stacking fault can also be described using the α-Si_3N_4 crystal structure.

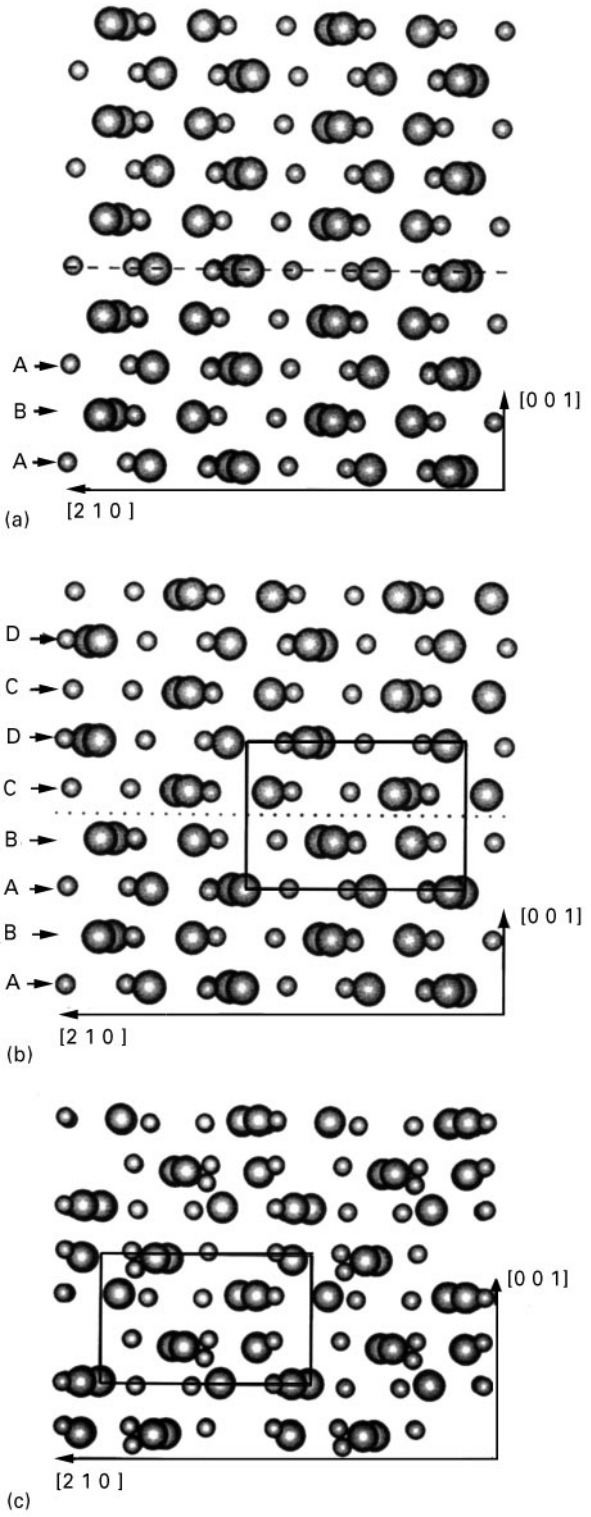

Figure 5 Schematic diagrams showing (a) the projection of the atomic structure of β-Si_3N_4 along [0 1 0], (b) the atomic construction of the stacking fault on a (0 0 1) plane, and (c) the projection of the atomic structure of α-Si_3N_4 along [0 1 0].

It should be noted here that the unit cell used for simulating the stacking fault has to have a longer ***a*** axis (vertical to the stacking fault plane) in order to avoid interference between the stacking faults in adjacent unit cells. We used the following unit cells: $a = 6.448$ nm, $b = 0.721$ nm and $c = 0.760$ nm for a stacking fault on the ($\bar{1}$ 0 1) plane, and $a = 5.822$ nm, $b = 1.318$ nm and $c = 0.760$ nm for a stacking fault

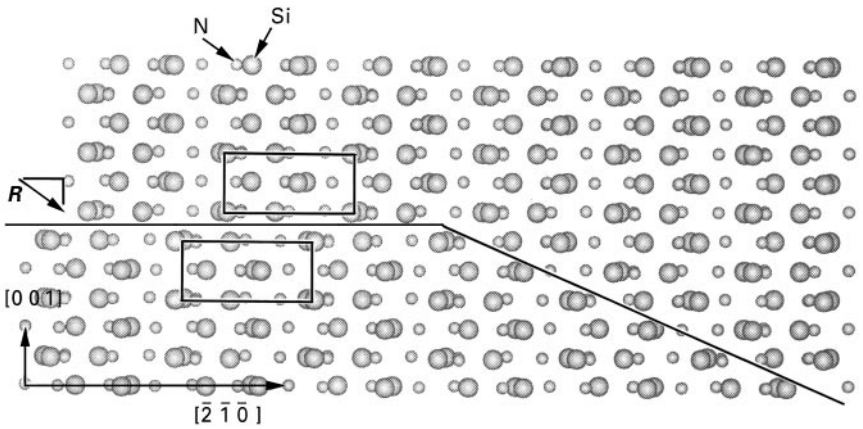

Figure 6 Schematic diagram showing the formation of the $\langle \bar{2}\,\bar{4}\,3 \rangle/6$ stacking fault continuously on the (0 0 1) and ($\bar{1}$ 0 1) planes without introduction of defects at the junction of the two planes. The projected translation vector ***R*** is marked.

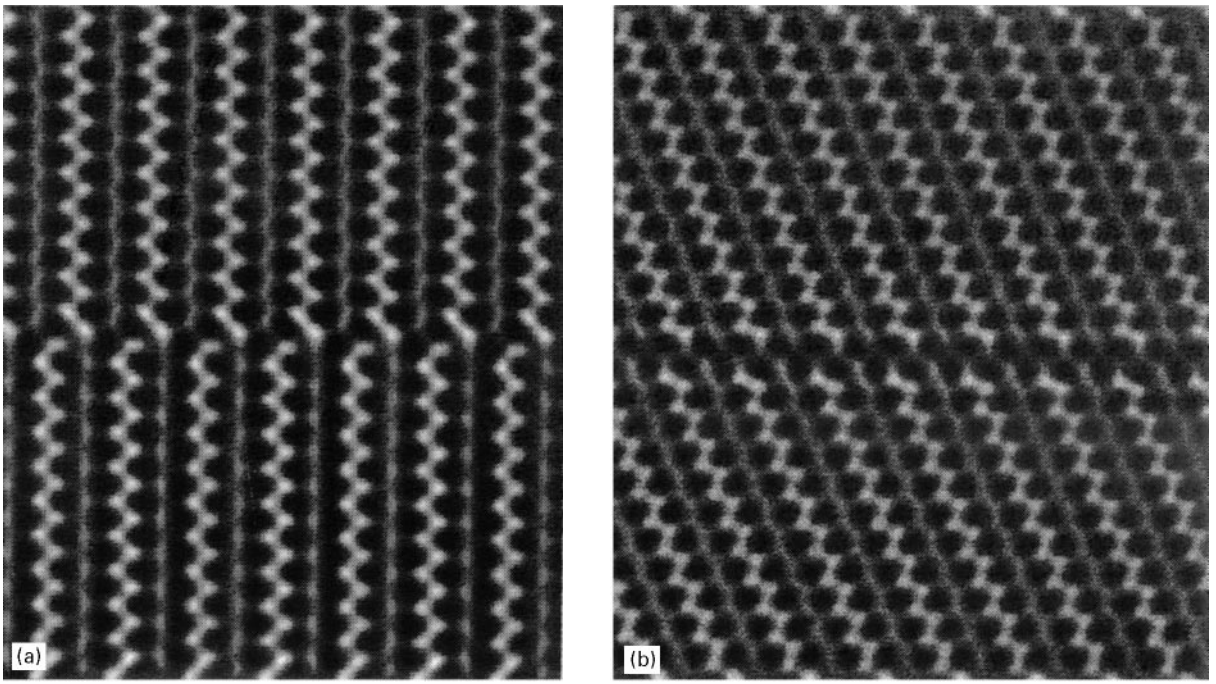

Figure 7 Simulated HRTEM images (a) of the stacking fault on the (0 0 1) plane seen in Fig. 4b, and (b) on the ($\bar{1}$ 0 1) plane seen in Fig. 4a.

on the (0 0 1) plane. Simulation for stacking faults on the ($\bar{1}$ 0 1) plane gave the results shown in Fig. 7b. Again, good agreement between the experimental and simulated images was found.

The transformation of one crystal type to another by the motion of sets of partial dislocations across the habit plane is best exemplified by the fcc → hcp phase transformation formed in metals such as cobalt. A similar mechanism could operate in the α-Si_3N_4 → β-Si_3N_4 transformation. The stacking sequence of ...ABCDABCD... (0 0 1) planes in α-Si_3N_4 can be transformed to the ..ABABAB... stacking sequence of β-Si_3N_4 by the motion of $\langle 4\,2\,3 \rangle/6$ partials across every second (0 0 1) plane. As Fig. 5 makes clear, small additional shuffles would be needed to bring the nitrogen atoms to their correct positions in the β unit cell. A stacking fault in β-Si_3N_4 represents an embryonic crystal of α-Si_3N_4, four atom planes in width. We believe that such a mechanism is the probable origin of the SFU characterized in this investigation, i.e. it is a manifestation of an incomplete reaction from α- to β-Si_3N_4 during the production of the whiskers.

4. Conclusion

Detailed analysis of a stacking fault formed on the (0 0 1) plane in a β-silicon nitride whisker indicates that it can be described by the α-Si_3N_4 crystal structure. The fault is thought to be formed by the α–β phase transformation during the whisker growth.

Acknowledgements

The authors are grateful for the support of an International Fellowship from the Natural Science and Engineering Research Council of Canada (XGN) and by a grant from National Natural Science Foundation of

China. X. G. N. also thanks Dr P. A. Stadelmann for his very kind help with the EMS program, Dr J. Pan, Changsha Institute of Technology, People's Republic of China, for specimen preparation, and Dr J. D. Embury, McMaster University, for useful discussions.

References

1. M. MITOMO and G. PETZOW, *MRS Bull.* **20**(2) (1995) 19.
2. F. F. LANGE, *J. Amer. Ceram. Soc.* **62** (1979) 428.
3. M. MITOMO, N. HIROSAKI and H. HIROTSURU, *MRS Bull.* **20**(2) (1995) 38.
4. K. KATO, Z. INOUE, K. KIJIMA, I. KAWADA, H. TANAKA and T. YAMANE, *J. Amer. Ceram. Soc.* **58** (1975) 90.
5. R. GRUN, *Acta Crystallogr.* **B35** (1979) 800.
6. P. GOODMAN and M. O'KEEFFE, *ibid.* **B36** (1980) 2891.
7. Y. BANDO, *ibid.* **B39** (1983) 185.
8. P. A. STADELMANN, *Ultramicroscopy* **21** (1987) 131.
9. X. G. NING, J. PAN, K. Y. HU and H. Q. YE, *Philos. Mag.* **A66** (1992) 811.
10. X. G. NING, J. PAN, K. Y. HU, H. Q. YE and H. FUKUNAGA, *J. Mater. Sci. Lett.* **11** (1992) 558.
11. J. HOMENY, L. J. NEERGAARD, K. R. HARASEK, J. T. DONNER and S. A. BRADLEY, *J. Amer. Ceram. Soc.* **73** (1990) 102.
12. S. AMELINCKX, in "Dislocations in Solids", edited by F. R. N. Nabarro, Vol. 2 (North-Holland, Amsterdam, New York, Oxford, 1979) pp. 67–460.
13. A. G. EVANS and J. V. SHARP, *J. Mater. Sci.* **6** (1971) 1292.
14. E. BUTLER, *Philos. Mag.* **21** (1971) 829.
15. P. M. MARQUIS, *J. Mater. Sci.* **12** (1977) 424.
16. W. E. LEE and G. E. HILMAS, *J. Amer. Ceram. Soc.* **72** (1989) 1931.

Received 19 April
and accepted 5 September 1996